Stiffness and surface topology of silicone implants competitively mediate inflammatory responses of macrophages and foreign body response

Sicen He [a],[1], Qingrong Zhang [a],[1], Jiezhi Jia [a], Wei Xia [a], Shengnan Chen [b],[c], Fanyi Min [b],[c], Yanlin Song [b],[c], Yunlong Yu [a],**, Jiangfeng Li [a],***, Zheng Li [a],*, Gaoxing Luo [a],****

[a] Institute of Burn Research, Southwest Hospital & State Key Lab of Trauma and Chemical Poisoning, Third Military Medical University (Army Medical University), Chongqing, 400038, PR China
[b] Key Laboratory of Green Printing, CAS Research/Education Center for Excellence in Molecular Sciences, Institute of Chemistry, Chinese Academy of Sciences (ICCAS), Beijing Engineering Research Center of Nanomaterials for Green Printing Technology, Beijing National Laboratory for Molecular Sciences (BNLMS), Beijing, 100190, PR China
[c] School of Chemistry and Chemical Engineering, University of Chinese Academy of Sciences, Beijing, 100049, PR China

ARTICLE INFO

ABSTRACT

Adverse inflammatory responses, dominated by macrophages, that are induced by physical cues of silicone implants can heavily damage the life quality of patients via causing fibrosis and device failure. As stiffness and surface topology affect macrophages at the same time, the competition or partnership among physical cues against the regulation of macrophages is still ambiguous. Herein, a series of PDMS implants with different stiffness at ~ MPa and surface topology at tens of micrometers were fabricated to investigate the relationship, the regulation rule, and the underlying mechanism of the two physical cues against the inflammatory responses of M1 macrophages. There is a competitive rule: surface topology could suppress the inflammatory responses of M1 macrophages in the soft group but did not have the same effect in the stiff group. Without surface topology, lower stiffness unexpectedly evoked stronger inflammatory responses of M1 macrophages. Implanting experiments also proved that the competitive state against mediating *in vivo* immune responses and the unexpected inflammatory responses. The reason is that stiffness could strongly up-regulate focal adhesion and activate the MAPK/NF-κB signaling axis to evoke inflammatory responses, which could shield the effect of surface topology. Therefore, for patient healthcare, it is crucial to prioritize stiffness while not surface topology at MPa levels to minimize adverse reactions.

1. Introduction

The development of modern medicine closely relates to the application of polymer biomaterials. Among these, silicone elastomers, such as polydimethylsiloxane (PDMS), have been widely used to fabricate medical devices for drug delivery, organ reconstruction, and prostheses in clinical treatments [1]. Numerous studies and applications have demonstrated that PDMS offers various advantages, including great biocompatibility, high oxygen permeability, good mechanical performance, excellent chemical stability, and easy surface patterning [2–4].

However, an increasing number of studies have indicated that unexpected immune responses, such as foreign body response (FBR), have heavily impaired the application of PDMS in patients' bodies over time. Excessive FBR can not only evoke a strong fibrosis process but also further induce pain and device failure, necessitating a second operation [5–8]. Therefore, it is urgent to overcome the FBR associated with implants.

Macrophages are a kind of innate immune cells, that play key roles in FBR and other biological processes such as wound healing and anti-pathogens [9–12]. Macrophages typically exhibit two classical

---

phenotypes: the classically activated phenotype (M1) and the alternatively activated phenotype (M2). Both of them have the same surface markers such as F4/80 and CD11b. Usually, macrophage phenotypes were divided by markers such as iNOS (Inducible Nitric Oxide Synthase) and CD86 (M1), and Arg-1 and CD206 (M2) [13,14]. M1 macrophages are involved in responding to FBR, by expressing various inflammatory cytokines and chemokines, including tumor necrosis factor-α (TNF-α), interleukin-1β (IL-1β), interleukin-6 (IL-6), and chemokine (C-C motif) ligand 2 (CCL2) [15]. After the acute inflammation, macrophages gradually differentiate into different polarization states. For example, M2a macrophages (a subtype of M2 macrophage) can express transforming growth factor-β (TGF-β) and interleukin-10 (IL-10) to regulate tissue repair and remodeling of extracellular matrix (ECM) in the final stage of wound healing [16,17]. Subsequently, activated fibroblasts, that is myofibroblasts, are recruited to the surfaces of implants, and then they largely express I-type collagen to form a fibrous capsule [18]. Therefore, the regulation against M1 macrophages has raised wide attention, such as modifying surface chemistry, surface topology, and stiffness of biomaterials [18–21]. Surface topology and stiffness are inherent material attributes that accompany the fabrication and post-treatment of biomaterials. These attributes can mimic the biophysical cues of ECM to directly regulate the viability, phenotype, and function of macrophages.

Previous studies have revealed that surface topology and stiffness can mediate the mechanical transduction to regulate the function of macrophages [21–24]. Surface topology can directly guide cell spreading and rearrange the cytoskeleton, further depressing the expression of inflammatory cytokines of M1 macrophages by tuning the myocardin-related transcription factor A (MRTF-A) into the nucleus [25]. On the other hand, stiffness not only mediates the cytoskeleton-related mechanical transduction by activating the downstream transcription factor Yes-associated protein (YAP) and transcriptional coactivator with PDZ-binding motif (TAZ) [26], but also changes Ca^{2+} influx through influencing ion channel Piezol [24]. Indeed, the Ca^{2+} influx can also assist the dephosphorylation process of YAP/TAZ to enhance YAP/TAZ into the nucleus [27], thus stiffness can mediate two mechanical sensors to activate the downstream transcription factor of YAP/TAZ. It shows that both surface topology and stiffness can mediate the cytoskeleton-related downstream transcription factors. However, they are capable of regulating different signaling molecules and altering the biological behavior of macrophages. Moreover, many studies have separately reported the importance of surface topology and stiffness in mediating macrophages; however, only a few studies have explored the real relationship or the underlying mechanism between surface topology and stiffness when they both affect macrophages at the same time. In addition, the stiffness-mediated mechanical transduction mainly focuses on hydrogels, which exhibit Young's modulus ranging from 1 to 280 kPa, significantly below the stiffness of ~2 MPa found in commercial PDMS implants [28,29]. Therefore, the regulation rule and mechanism of M1 macrophages on high stiffness PDMS substrates, and even the relationship between surface topology and stiffness are still ambiguous.

Herein, we fabricated various PDMS substrates with different stiffness and surface topographies to investigate the inflammatory responses of M1 macrophages. To be consistent with clinical application, the Young's modulus of PDMS was adjusted to 0.5 and 1.5 MPa, which is close to that of commercial silicone implants (~2 MPa) [27]. The surface topology of PDMS was designed as stripe arrays and dot arrays matching the size of a single macrophage. Utilizing immunofluorescence, real-time quantitative polymerase chain reaction (RT-qPCR), flow cytometry, histology, and RNA-sequencing (RNA-seq) techniques, we found that surface topology and stiffness were in a competitive relationship. At the stiffness levels of MPa, the stiffness dominated and enhanced the inflammatory responses of M1 macrophages with the decrease of stiffness, which evoked a stronger fibrosis process. In contrast, the surface topology showed a weak depression to M1 macrophages. Both mechanical signals, stiffness, and topology, affect the

activity of NF-κB in the late response of macrophages, thereby causing differences in the expression of late proinflammatory factors.

2. Results

2.1. Material properties of PDMS substrates with different stiffness

We first fabricated biocompatible PDMS substrates (stiff and soft) with various moduli at the level of ~MPa by tuning the ratio between the base component and the curing component (Fig. 1a and Materials and Experiments). The stress-strain curves showed that stiff and soft PDMS could reach the maximum strain of about 155 % and 230 %, and the toughness of 4.1 MPa and 0.89 MPa, respectively (Fig. 1b). Their Young's modulus were about 1.5 and 0.5 MPa, respectively (Fig. 1c). Accompanying the differences in Young's modulus, stress-releasing behaviors were also distinct. Soft PDMS could quickly release the stress to nearly 8 % during the first 3 h under the pre-strain of 10 %, while the stiff one needed about 6 h to reach the biggest release of about 7 % under the same condition (Fig. S1). Thus, the mechanical properties between soft and stiff PDMS showed a significant difference. Besides, surface properties including wettability, component, and roughness all could affect cell adhesion to materials, and even tune the function and phenotype of cells [21,30,31]. Therefore, we further investigated their surface properties via contact angle instrument, X-ray photoelectron spectroscopy (XPS), and atomic force microscope (AFM). Fig. 1d and e showed that the mean contact angles of water droplets on the stiff and soft PDMS substrates were 117° and 119°, respectively. On the other hand, the mechanical properties of PDMS were adjusted by the crosslinking ratio, which may change the ratio of -OH by -CH₃. Previous studies had proved that surface chemical components could mediate the protein absorption such as fibronectin and collagen which tuned cell adhesion [32]. XPS results demonstrated that chemical components of Si, C, and O were consistent in two substrates, they were about 45 %, 29 %, and 26 %, respectively (Fig. 1f–g, Fig. S2, and Table S1). Especially, the peak of O 1s in different substrates had no differences. Surface topology also could significantly affect cell behaviors, thus the surface micro-topology of PDMS substrates was characterized by AFM. The morphology images showed that both stiff and soft PDMS substrates exhibited porous structures in the diameter of about 25 nm, the cross profiles of about ±10 nm, and the roughness of Ra = 5.78 and 6.46 nm, respectively (Fig. 1h and i). Therefore, experimental results proved that tuning crosslinking ratios only changes the mechanical properties of PDMS but does not impact the wettability, surface components, and roughness. Thus, stiffness is the unique variable among PDMS substrates.

2.2. Inflammatory responses of M1 macrophages to PDMS with variable stiffness and surface topology

Relying on the unique material properties of PDMS, we fabricated patterned PDMS substrates with tunable stiffness to explore the relationship between stiffness and surface topology in mediating inflammatory responses of macrophages. We used murine bone marrow-derived macrophages (BMDMs) from wild type C57BL/6 mice to explore the regulation effect of stiffness and surface topology. Unstimulated BMDMs showed the same morphology independent of stiffness, with the spreading area of about 850 μm² and an aspect ratio of 1.5 (Fig. S3). To tune the single BMDM, two classical patterned PDMS substrates were fabricated by capillary printing, including stripe arrays and dot arrays based on the previous studies [33,34] (Figs. S4–5 and Fig. 2a). 3D microstructures were captured by the white light interferometer, showing the line width of 10 μm and the center-to-center line distance of 20 μm in the stripe arrays, and the dot diameter of 20 μm and the center-to-center dot distance of 30 μm in the dot arrays, characteristic height was 5 μm, as shown in Fig. 2b and c.

Here, PDMS substrates were divided into stiff and soft groups, and
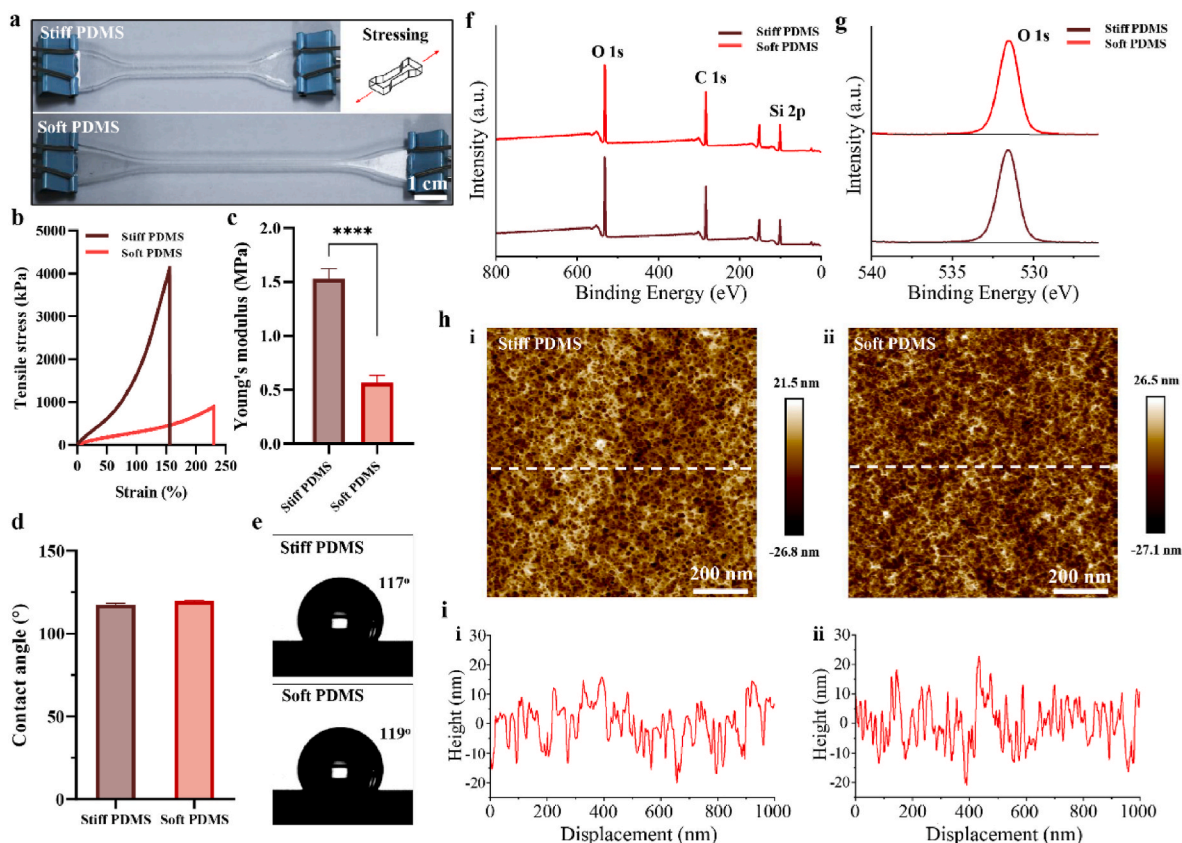
Fig. 1. Material properties of PDMS substrates. (**a**) Pictures of the stiff and soft PDMS substrates under the same stress. Inset: the stretching process. (**b**) Stress-strain curves of the PDMS substrates. (**c**) Young's modulus of the PDMS substrates. $n = 5$. (**d**) Contact angles of the PDMS substrates. $n = 3$. (**e**) Images of water droplets on the PDMS substrates, corresponding to (d). (**f**) XPS diagram of the PDMS surfaces. (**g**) Amplified XPS diagram of O1s. (**h**) AFM images of the stiff (i) and soft (ii) PDMS surfaces in $1 \times 1 \ \mu m^2$. (**i**) Profile diagrams of the stiff (i) and soft (ii) PDMS surfaces corresponding to white dash lines in (h). Bars denote Mean $\pm$ SD, ****$p < 0.0001$ as determined by Two-way ANOVA and Tukey post-hoc test.

each group contained junior sets: flat, stripe arrays, and dot arrays. Before culturing BMDMs, PDMS substrates were first coated with fibronectin at 37 °C. Topological microstructures could tune cell spreading to change the morphology of M1 BMDMs stimulated with lipopolysaccharide/interferon-γ (LPS/IFN-γ). After stimulating BMDMs with LPS/IFN-γ for 24 h, the immunofluorescence images of M1 BMDMs were captured by laser scanning confocal microscopy (LSCM). In contrast to completely spreading on flat PDMS, stripe arrays and dot arrays could confine the cytoskeleton of M1 BMDMs, forming an elongated state and a contracted state, respectively (Fig. 2d). Subsequently, we quantitatively analyzed the cell spreading area, the nucleus projected area, and the aspect ratio of cells and cell nuclei. The cell spreading area followed the order of flat group > stripe group > dot group, while the cell elongation in the stripe group reached up about 5.0 which was significantly higher than that in the flat and dot groups. Notably, the difference in stiffness didn't cause a significant change in cell spreading area and elongation (Fig. 2e and f). The cell spreading area was about 500 μm² on the dot-array substrates, which was far below that on the flat substrates (1150 μm²), even smaller than M0 BMDMs on the flat substrates (850 μm²), showing the strongest confinement effect (Fig. 2e and Fig. S3b). Although the stripe-array substrate could also confine cell spreading, its confinement effect was also much weaker than the dot-array substrate. Therefore, the cytoskeleton was directly regulated by surface topology. Moreover, the nucleus may also be influenced by stiffness or surface topology. Therefore, we also analyzed the nuclear area and elongation, where the nuclear area on stripe arrays and dot arrays showed a decreasing trend similar to that of the cytoskeleton. However, the relative nuclear area in stiff stripe and dot arrays did not follow the cytoskeletal changes. Due to the

average nucleus area being far below the cytoskeleton area, the differences in the nucleus area among groups were less significant than those in the cytoskeleton area (Fig. 2g). As shown in Fig. 2h, the rule of nucleus elongation was consistent with that of cytoskeleton elongation on both stiff and soft PDMS. Considering the size of the nucleus is generally smaller than that of the microstructure, it is not directly regulated by the microstructure in most cases. Besides, the influence of stiffness on the nucleus must depend on the cytoskeleton and the LINC (linker of the nucleoskeleton to the cytoskeleton) complex [35]. We could conclude that stiffness and surface topology can indirectly affect the morphology of the nucleus through the mechanical transduction of the cytoskeleton in our study. Therefore, the cytoskeleton played a core role in nucleus regulation originating from physical cues. Moreover, the morphologies of macrophages were closely related to their function and phenotype, which have been demonstrated by previous studies through the confinement effect of topological structures [24,25]. Next, we explored the inflammatory responses of M1 macrophages related to stiffness and surface topology via immunofluorescence, flow cytometry, RT-qPCR, and ELISA.

First, the classical marker of M1 macrophages, iNOS, was characterized by the immunofluorescence technique. Fig. 3a showed that the expression of iNOS could be suppressed with the assistance of smaller stiffness and confinement, proving that the expression of iNOS was dependent on surface topology and stiffness. The semiquantitative analysis of mean fluorescence intensity (MFI) of iNOS unveiled that surface topology can play roles either on stiff PDMS substrates or on soft PDMS substrates, among them the dot arrays exhibited the strongest inhibition to M1 macrophages (Fig. 3b). According to immunofluorescence images of the single BMDM on various substrates, the expression
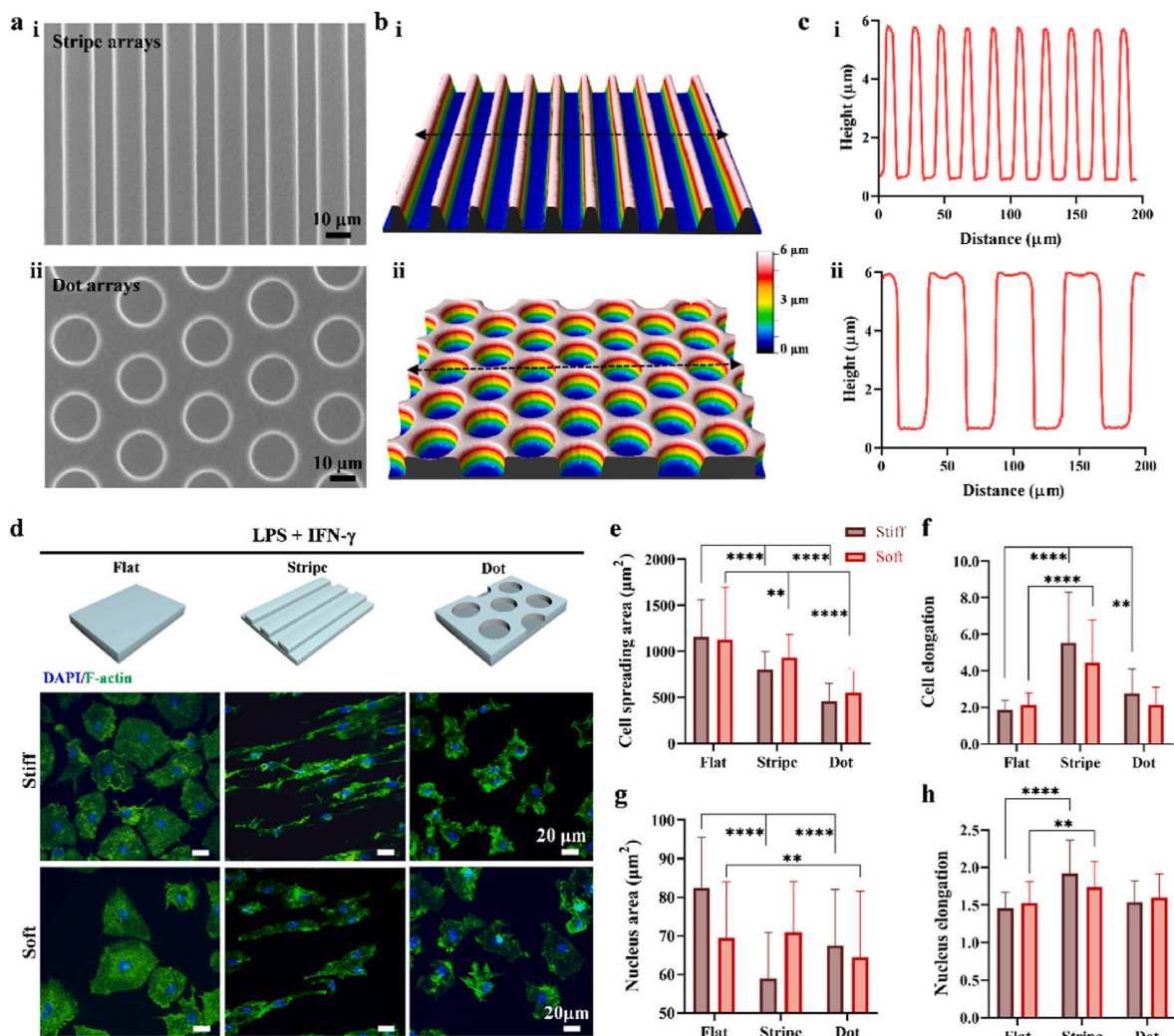
Fig. 2. Morphology of M1 BMDMs on patterned PDMS substrates. (**a**) Scanning electron microscopy (SEM) images of stripe-array (**i**) and dot-array (**ii**) PDMS substrates. (**b**) 3D profiles of stripe-array (i) and dot-array (ii) PDMS substrates corresponding to (a). (**c**) Cross-profile diagrams of microstructures on stripe-array (i) and dot-array (ii) PDMS substrates, corresponding to black double-arrow lines in (b). (**d**) Fluorescence images of M1 BMDMs on PDMS substrates with different topologies and Young's moduli. Blue denotes nucleus and green denotes F-actin. (**e**) Cell spreading area of M1 BMDMs on different PDMS substrates. $n = 100$. (**f**) Cell elongation of M1 BMDMs on different PDMS substrates. $n = 100$. (**g**) Nucleus area of M1 BMDMs on different PDMS substrates. $n = 200$. (**h**) Nucleus elongation of M1 BMDMs on different PDMS substrates. $n = 200$. Bars denote Mean $\pm$ SD, $*p < 0.05$, $**p < 0.01$, $***p < 0.001$ as determined by Two-way ANOVA and Tukey post-hoc test. (For interpretation of the references to colour in this figure legend, the reader is referred to the Web version of this article.)

of iNOS and the shape of the cytoskeleton were closely related (Fig. S6). The cytoskeleton of M1 macrophages on stripe and dot arrays had been changed via surface topology, and the corresponding expression of iNOS was depressed significantly. The results also unveiled that dot arrays could inhibit the spreading of the cytoskeleton of M1 macrophages stronger than stripe arrays, independent of the substrate's stiffness. The differences between stripe arrays and dot arrays mainly originated from the distribution of microstructures, which also followed the previous study about the confined space effect of topology [24]. Therefore, the spreading of the cytoskeleton could directly mediate the expression of iNOS. Furthermore, to more accurately evaluate the relative expression of iNOS, we used flow cytometry to show that the ratio and MFI of iNOS$^+$ cells had been strongly depressed by surface topology, special the dot arrays which was consistent with immunofluorescence experiments (Fig. S7). Moreover, the regulatory effect originating from stiffness seemed not to work. Therefore, only surface topology could significantly suppress the expression of iNOS, and stiffness seemed not to cooperate with surface topology to reach a stronger inhibition effect as we expected.

Next, the ratio of M1 macrophages on various substrates was

characterized by flow cytometry to analyze the evolution law of phenotype. CD86 and CD206 were used as the characteristic marks in flow cytometry. For BMDMs used in this study, M0 macrophages located at the region of CD206$^-$CD86$^-$ cells (63.7 %), M1 macrophages mainly located at the region of CD86$^+$CD206$^-$ cells (44.6 %), while M2 macrophages included CD86$^+$CD206$^-$ and CD86$^+$CD206$^+$ cells (35.3 %) (Fig. S8). As shown in Fig. 3c, the flat PDMS in the stiff group exhibited the highest ratio of CD86$^+$CD206$^-$ cells about 43.7 %, while the dot-array PDMS in the soft group expressed the lowest ratio of about 35.1 %. Quantitative analysis showed that the dot-array PDMS in the stiff and soft groups unveiled the strongest depression against the ratio of M1 macrophages, but the inhibition effect resulting from stiffness was negligible (Fig. 3d). Therefore, the ratio of M1 macrophages was strongly dependent on surface topology, which was consistent with the expression of iNOS.

To deeply analyze the function of M1 macrophages tuned by stiffness and surface topology, the marked inflammatory genes of *Nos2*, *Tnf*, *Il6*, and *Il1b* were measured via RT-qPCR. Based on the expression of mRNA relative to GAPDH, we found that the trend in *Nos2* was almost consistent with that of immunofluorescence, but the other inflammatory genes
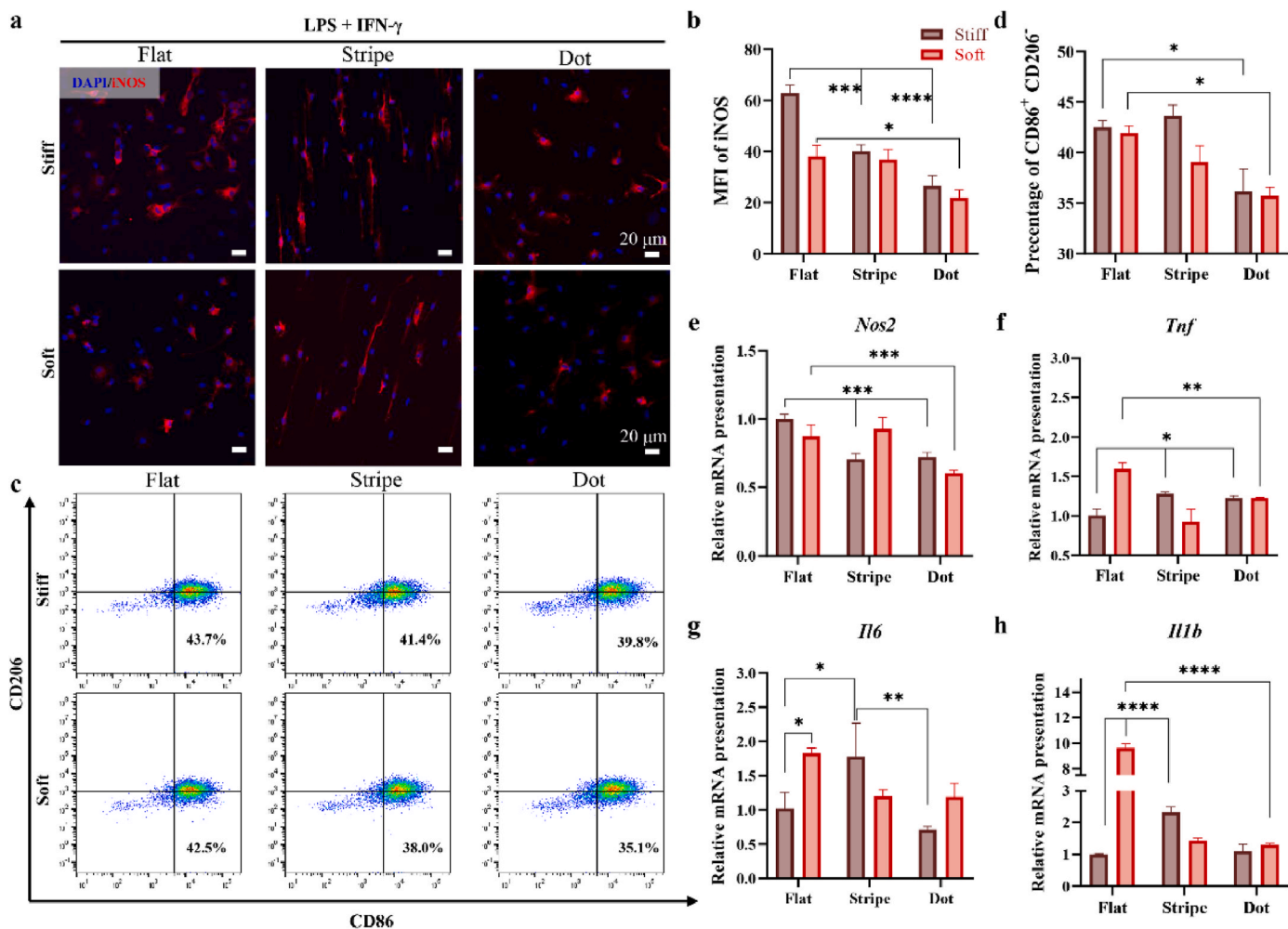
Fig. 3. *In vitro* **inflammatory responses of M1 BMDMs to stiffness and surface topology.** (**a**) Immunofluorescent images of iNOS in M1 BMDMs on different PDMS substrates. Red and blue denote iNOS and nucleus, respectively. (**b**) MFI diagram of iNOS corresponding to (a). (**c**) Flow cytometry of CD86$^+$ BMDMs on different substrates. (**d**) The percentage of CD86$^+$CD206$^-$ BMDMs to all BMDMs on various substrates. (**e-h**) Relative expression of inflammatory genes *Nos2* (e), *Tnf* (f), *Il6* (g) and *Il1b* (h). $n = 3$. Bars denote Mean ± SD, *$p < 0.05$, **$p < 0.01$, ***$p < 0.001$, ****$p < 0.0001$ as determined by Two-way ANOVA and Tukey post-hoc test. (For interpretation of the references to colour in this figure legend, the reader is referred to the Web version of this article.)

showed a more complicated rule, where the soft substrate unexpectedly upregulated the expression levels of *Tnf, Il6,* and *Il1b* (Fig. 3e–h). The quantitative results showed that the expression level of *Nos2* was mainly tuned by the surface topology of the substrate, while weakly related to the stiffness. The reason may be that iNOS was directly tuned by the downstream signaling molecules of the cytoskeleton. Other inflammatory genes like *Tnf, Il6,* and *Il1b* may be strongly tuned by the mechanical transduction resulting from the stiffness of the substrate. In the stiff group, stripe arrays consistently evoked the up-regulation of Tnf, Il6, and Il1b, whereas dot arrays exhibited weak regulatory effects against them. Conversely, all topological substrates significantly down-regulated the inflammatory genes in the soft group. However, no significant differences were observed among stripe arrays and dot arrays. In the soft group, the down-regulation effect of surface topology against M1 macrophages was consistent with previous reports [24,25]. Besides, different from previous studies [25,36], the decrease in stiffness unexpectedly evoked the up-regulation of inflammatory genes in our study. The phenomenon may originate from the different mechanical properties of PDMS, such as the high stiffness at the levels of 1 MPa which was 10~1000 times bigger than the hydrogels (Young's modulus of 1–280 kPa) used in studies. Subsequently, we further measured the downstream inflammatory cytokines (TNF-α and IL-6) to demonstrate how the function of M1 macrophages is mediated by stiffness and surface

topology. ELISA experiments showed that the expressions of both TNF-α and IL-6 could be significantly depressed by dot arrays in both stiff and soft groups, while they were not changed by stiffness as that at the gene levels (Fig. S9). In contrast, dot arrays played stable regulation effects no matter at gene or protein levels.

In summary, at the stiffness level of MPa, both stiffness and surface topology can regulate the late inflammatory responses of M1 macrophages at the gene level, but they follow different laws. For flat substrates, soft PDMS could up-regulate inflammatory genes compared to stiff PDMS. For patterned substrates, stiffness did not cause differential expressions at the gene level. When we only focused on surface topology, dot arrays exhibited the strongest inhibition effect against M1 macrophages in either the stiff group or the soft group, which was consistent with the rule of cell spreading area. The expression of downstream cytokines further verified the basic law depending on the confined space effect. We hypothesized that the nucleus translocation of the transcription factor NF-κB at the early stage may be mediated by the substrates with various stiffness and surface topologies. To verify the above hypothesis, we further explored the nuclear translocation of NF-κB (p65) in macrophages on various substrates after being stimulated by LPS/INF-γ for 1 h. Immunofluorescence images indicated that the nuclear translocation of p65 did not significantly change with the stiffness and surface topology of the substrates in the first few hours

(Figs. S10a–b). Furthermore, we utilized Western Blot to measure the ratio of p-p65 (located in the nucleus) to p65 (located in the cytoplasm) on different substrates. The results were consistent with the immunofluorescence images showing that NF-κB was not impacted by stiffness and surface topology at the early stage (Figs. S10c–d). On the one hand, the previous study [24] revealed that the activity of NF-κB in the nucleus can be mediated by other transcription factors at the late stage (6 h later after adding stimulators). On the other hand, both the inflammation-related gene expression and inflammatory cytokines were tested at 24 h after being stimulated by LPS/INF-γ, which is at the late stage. To further investigate the late expression of inflammatory genes in macrophages and the signaling pathways involved, we conducted RNA-seq to analyze the gene expression of macrophages after 24 h.

### 2.3. Mechanism of inflammatory responses of macrophages to stiffness and surface topology

Since the uniformity of chemical components, micro-topology, and roughness among different groups, stiffness, and surface topology are the only two variables. Indeed, both stiffness and surface topology can directly tune the cytoskeleton and cell membranes, which means that they can influence the mechanical transduction based on the cytoskeleton and ion channel. However, stiffness, differing from surface topology, can activate integrin and downstream signal molecules such as focal adhesion kinase (FAK), talin, vinculin, and src [27], and finally may mediate mechanical-sensitive transcription factor YAP/TAZ to regulate the NF-κB signaling pathway. Increasing studies have shown that the mechanical properties of materials can affect cell functions via viscoelasticity or stiffness, inducing complex regulation laws [37–39]. To understand the underlying mechanism of immune regulation from stiffness and surface topology and the underlying relationship between stiffness and surface topology. Gene expression of M1 macrophages in Stiff, Soft, and Soft Dot-Array (Soft_D) groups was conducted via RNA-seq analysis. Principal Component Analysis (PCA) of genes among Stiff, Soft, and Soft_D groups showed that the differences caused by stiffness were significant, while the differences caused by surface topology could be ignored (Fig. 4a). Volcano plots of differentially expressed genes quantitatively presented the up-regulated and down-regulated genes among Soft *vs* Stiff, Soft_D *vs* Stiff, and Soft_D *vs* Soft (Fig. 4b). Both Soft *vs* Stiff and Soft_D *vs* Stiff showed significant expression differences in genes where differential genes reached up to 612 (up) and 377 (down), and 582 (up) and 429 (down), respectively. When we only focused on the effect of surface topology (Soft_D *vs* Soft), the significantly differential genes were reduced to 14 (up) and 24 (down), indicating that the regulatory effect of surface topology was negligible. Therefore, the mechanical properties of PDMS were dominant in regulating BMDMs, consistent with the experimental results mentioned above. Given that Young's modulus is at the MPa range, we hypothesize that the mechanical transduction mediated by stiffness exceeds that mediated by surface topology.

Subsequently, we further analyzed the differentially expressed genes among groups via a heat map, setting the Stiff group as the control group. As shown in Fig. 4c, typical inflammatory genes such as *Il1b*, *Tnf*, *Il6*, *Nfkb2*, *Ccl3,* and *Tlr2* were significantly up-regulated in the Soft_D and Soft groups, meanwhile, adhesion, cytoskeleton, and mechanical transduction-related genes such as *Itga1*, *Itgb1*, *Rho*, *Src*, *Acta2*, and *Tln1* were up-regulated in the Soft_D and Soft groups as well. The down-regulated genes in the Soft_D and Soft groups, including *Nos2*, *Ccl2*, *Ccl5*, *Ccl7*, and *Ccl12*. Besides, classical mechanical transduction genes such as *Yap1* and *Piezo1* did not change significantly. Thus, adhesion and cytoskeleton should play important roles in the inflammatory responses of M1 macrophages. Since there are no differences between the Soft group *vs* Soft_D group, then we mainly focused on the comparison between the soft group and the stiff group via Gene Ontology (GO) enrichment analysis, which showed that cell adhesion, inflammatory response, and signal transduction were in the top GO enrichment

(Fig. 4d). The results denoted that the relationship between cell adhesion and immune response was key for explaining immune responses related to the mechanical properties of materials. To figure out the underlying mechanism, the Kyoto Encyclopedia of Genes and Genomes (KEGG) signaling pathway was conducted to show the top signaling pathways. As illustrated in Fig. 4e, the focal adhesion signaling pathway, the MAPK signaling pathway, the PI3K-AKT signaling pathway, and the NF-κB signaling pathway were identified in the top KEGG enrichment. The results of GSEA further indicated that the NF-κB pathway was significantly up-regulated at the late stage due to the soft substrate (Fig. S11). Indeed, the focal adhesion can mediate the MAPK signaling pathway or the PI3K-AKT signaling pathway, both of which could further modulate the NF-κB signaling pathway [40]. We analyzed the relative expression of key genes involved in these signaling pathways, as shown in Fig. 4f. Adhesion and mechanical transduction-related genes such as *Itga5*, *Itgb1*, *Src*, and *Vc* were significantly up-regulated in the soft group, *Mrtfa* was significantly down-regulated, while the change of *Piezo1* could be ignored. Src kinase is also involved in the downstream signal transduction of Toll-like receptor 4 (TLR4) to activated MAPKs [41]. Therefore, we compared the MAPK and PI3K-Akt-related genes in the stiff and soft groups, including *Junb* (AP-1), *Mapk1* and *Mapk14* (p38), *Pik3r1* and *Pik3cd* (PI3K), and *Akt1*. Among them, only AP-1 was significantly up-regulated in the soft group, compared to the stiff group. Furthermore, we built the signaling pathway interaction networks, as shown in Fig. 4g. The networks indicated that the MAPK signaling pathway directly connected to focal adhesion and the NF-κB signaling pathway at the same time, while the PI3K-AKT signaling pathway indirectly linked with the NF-κB signaling pathway via interacting with the TNF signaling pathway and the Toll-like receptor signaling pathway. Besides, in the soft group, the presence of dot arrays didn't activate any new function and signaling pathway (Fig. S12), proving that surface topology was a secondary regulatory factor in contrast to stiffness. Therefore, combining RT-qPCR and RNA-seq results, we could conclude that the activated M1 macrophages on the softer substrates up-regulated integrin and src, which could evoke stronger and more persistent inflammatory responses (Fig. 4h) by activating the downstream molecules AP-1 of the MAPK signaling pathway [42] that may affect the NF-κB activity at the late stage, and finally up-regulated inflammation-related genes. Moreover, since the same mechanical transduction pathway (cytoskeleton) was involved, the competition between stiffness and surface topology determined the final response of M1 macrophages, and obviously, stiffness dominated the inflammatory genes transcription of M1 macrophages on the hard material at the stiffness levels of MPa (Fig. 4i).

2.4. In vivo immune responses to stiffness and surface topology

To explore the role of stiffness and surface topography in the immune responses *in vivo*, PDMS implants were put into the dorsal skin of rats, since the ratio of macrophages could be more than 50 % during the first 28 days post-implantation [43]. The PDMS implants with different stiffness and surface topology were cut into discs (Φ 6 mm × 2 mm thick) which were separately inserted into the rats' backs, within the fascia tissue overlying the dorsal skeletal muscle on day 0. They were then excised along with the surrounding tissues on days 3 and 14 post-implantation (Fig. 5a). To verify the inflammatory responses of immune cells to stiffness and surface topology, implants with surrounding tissues were processed for histology by hematoxylin and eosin (H&E) staining, Masson's trichrome staining, and immunofluorescence. H&E images of skin tissues on days 3 and 14 denoted the evolution of acute inflammation responses in every group. On day 3, the inflammatory level showed significant differences among groups, which were tuned by stiffness and surface topology. In the stiff groups, surface topology including stripe arrays and dot arrays, induced higher inflammation levels than the flat surface (Fig. S13a). On the contrary, the inflammatory level in the soft group was independent of surface
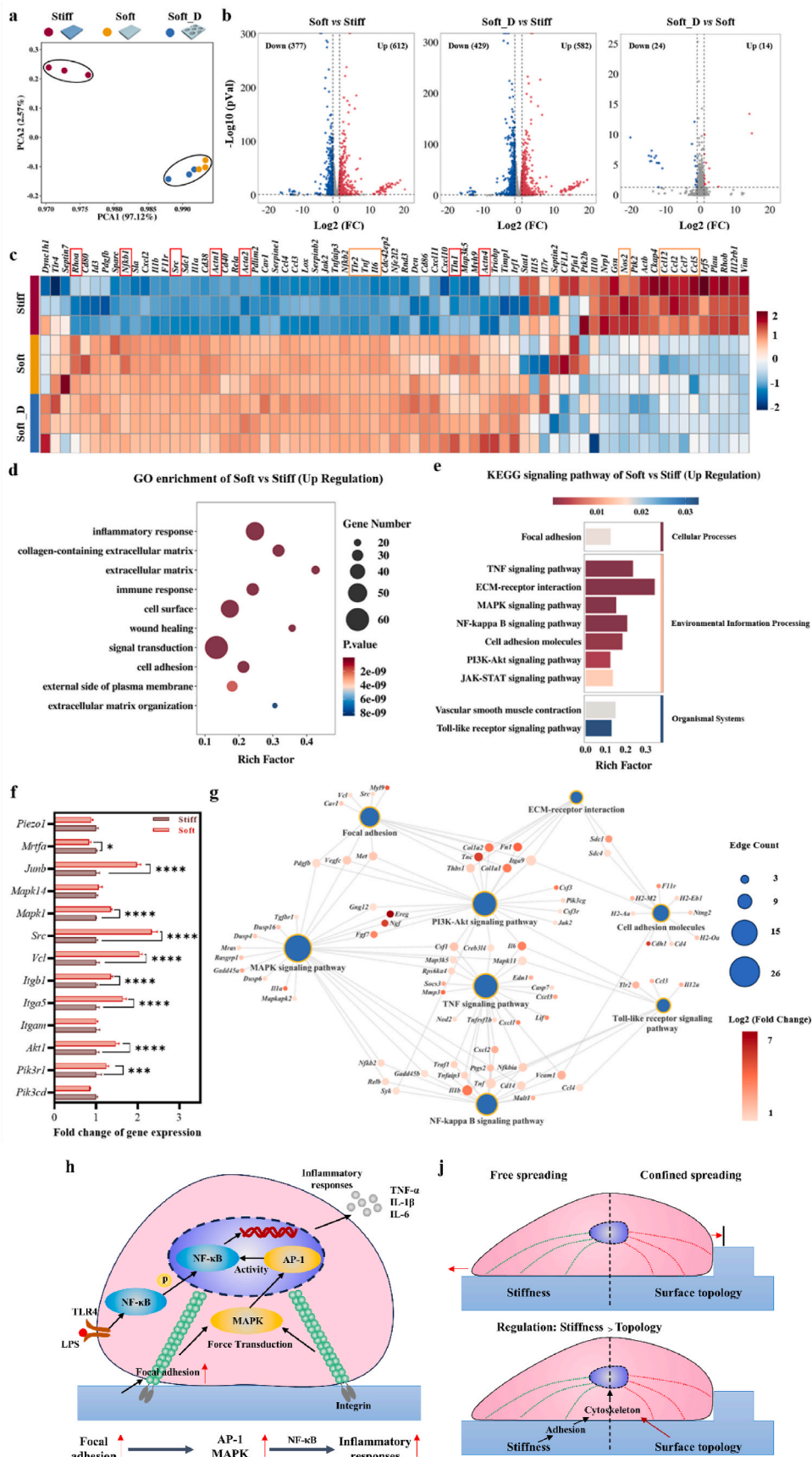
(caption on next page)

Fig. 4. Regulation mechanism of mechanical factors to M1 macrophages. (**a**) PCA analysis of differentially expressed genes on stiff, soft, and soft-D PDMS substrates. (**b**) Volcano plots of differentially expressed genes on different PDMS substrates. (**c**) Heat map of differentially expressed genes on different PDMS substrates (*n* = 3). (**d**) GO enrichment of soft PDMS *vs* stiff PDMS. (**e**) KEGG signaling pathway enrichment of soft PDMS *vs* stiff PDMS (*n* = 3). (**f**) Fold change of gene expression involving in focal adhesion, MAPKs, and mechanical transduction (*n* = 3). (**g**) Signaling pathway interaction networks of soft PDMS *vs* stiff PDMS. (**h**) The possible underlying mechanism of inflammatory responses of M1 macrophages mediated by stiffness. (**i**) Schematic of the competitive relationship between stiffness and surface topology.

topology, as the flat surface, stripe arrays, and dot arrays exhibited a similar level of inflammation (Fig. S13a). Since inflammatory cell infiltration could reflect the local inflammatory level, the cell density surrounding implants was measured. The cell density followed the order of dot (3340 mm^{-2}) > stripe (1893 mm^{-2}) > flat (1416 mm^{-2}) in the stiff PDMS group, while the cell density of dot ≈ stripe ≈ flat was about 2900 mm^{-2} in the soft PDMS group (Fig. S13b). The results demonstrated that the soft implants could evoke more severe immune responses on day 3 post-implantation and shield the regulation effect of surface topology at the same time.

On the 14th day post-implantation, the inflammation cells around the implants sharply decreased to be negligible, which was independent of the stiffness and surface topology of implants (Fig. 5b). Subsequently, we analyzed the cell density of surrounding tissues near to implants to reflect the inflammatory level. The cell density sharply decreased to 150-300 mm^{-2}, and the differences among implants became inappreciable in the stiff group, while the dot arrays in the soft group were significantly higher than the others (Fig. 5c). To further understand the long-term immune response mediated by stiffness and surface topology, we analyzed Masson's trichrome images of skin tissues on day 14. As shown in Fig. 5d, topological implants caused thinner capsules than flat implants in the soft group but did not work in the stiff group. The thickness in the soft flat group was larger than that in the stiff flat group. The soft dot arrays showed the thinnest capsule thickness of about 58 μm, half of 117 μm in the soft flat group, but with a slightly higher level of collagen density (Fig. 5e and Fig. S14). The results indicated that soft dot arrays could play a role in suppressing the inflammatory responses of immune cells after 3 days.

The role of macrophages during implantation was analyzed by immunofluorescence. M1 macrophages were marked by F4/80 and CD68 on days 3 and 14. The fluorescence intensity of CD86 on day 3 was higher than that on day 14, and it was independent of stiffness and surface topology (Fig. 5f). Based on quantitative analysis of F4/80$^+$ (macrophages) and F4/80$^+$CD86$^+$ (M1 macrophages) cells on day 3, the ratios of macrophages and M1 macrophages were at the same level among groups, independent of stiffness and surface topology (Fig. 5g and h). After 14 days, although the ratios of F4/80$^+$ and F4/80$^+$CD86$^+$ cells were similar to that on day 3, the total macrophages had decreased sharply relative to them on day 3. The ratio of macrophages in the stiff group (about 0.35) was slightly higher than that in the soft group (about 0.3), but independent of surface topology, meaning that stiffness may dominate the recruitment of macrophages (Fig. 5i). Moreover, the ratio of M1 macrophages associated with surface topology only revealed significant differences in the soft group, showing a marked increase of up to 0.6 in the surface topology (Fig. 5j). It showed that the stiffness of implants was the prerequisite for the surface topology to play a role, and stiffness and surface topology were in a competitive state, which was consistent with the *in vitro* experiments (Fig. 3). According to the *in vitro* experiments, we expected that the ratio of M1 macrophages should decrease with surface topology in the soft group, however, there was an increase with surface topology. We suspected that there are two reasons: 1. The fibrous process involving macrophages, neutrophils, and fibroblasts etc [44], thus the crosstalk between cells makes the results complicated. 2. ECM may play an important role in the mechanical transduction against implants [18]. Although the ratio of M1 macrophages didn't match our expectations, the change of capsule thickness indicated that the relationship between stiffness and surface topology also applies to immune responses *in vivo*.

3. Discussion and conclusion

In recent two decades, biophysical cues that strongly mediate proliferation, adhesion, polarization, and phenotype of cells have increasingly attracted the attention of researchers and doctors [6,18,31,45,46]. Both stiffness and surface topology can mimic the biophysical cues of the ECM, and they are inherent physical attributes of biomaterials accompanying their production. Several studies focused on the impact of stiffness and surface topology on macrophages, but similar and contradictory conclusions have been drawn. An accepted fact is that no matter stiffness or surface topology can depress inflammatory responses of M1 macrophages [47,48]. Therefore, stiffness and surface topology may have a synergistic effect on inhibiting M1 macrophages and inhibiting FBR. For silicone implants, stiffness and surface topology have been separately studied in mediating FBR processes [18,27]. However, the comprehensive effect on M1 macrophages resulting from both stiffness and surface topology has never been explored.

Using mechanically adjustable material, PDMS, the comprehensive regulation by stiffness and surface topology was investigated. When the Young's modulus is at the levels of MPa, stiffness and surface topology could play different roles in the regulation of M1 macrophages. According to RT-qPCR experiments, gene expressions of inflammatory cytokines showed that the regulation effect of surface topology was strongly dependent on the stiffness of substrates, where the inhibition of inflammatory responses of M1 macrophages resulting from surface topology only happened on the soft PDMS substrates (0.5 MPa), while it could result in an opposite effect on the stiff PDMS substrates (1.5 MPa). Based on ELISA results, the downstream protein expressions of inflammatory cytokines followed the similar rule that surface topology depressed the inflammation. However, the evoked genes on the soft flat substrate did not significantly mediate the downstream cytokines expression. In words, dot arrays exhibited the strongest inhibition of M1 macrophages among all groups, which is consistent with the previous study [6]. Furthermore, we used subcutaneous implanting experiments to verify the regulation rule resulting from stiffness and surface topology based on the acute inflammatory responses. Due to the complexity of real immune microenvironment, we found that surface topology could induce stronger inflammatory responses in the stiff group during the acute inflammatory stage (the 3rd day), while it did not cause significant differences in the soft group. Besides, for flat substrates, the lower stiffness evoked stronger inflammatory responses *in vivo*, which was consistent with the *in vitro* experiments. Therefore, *in vivo* acute inflammatory responses partially followed the *in vitro* experiments, since the other immune cells also played roles during the stage. *In vitro* and *in vivo* experiments both demonstrated that stiffness and surface topology did not work together to depress inflammatory responses of M1 macrophages, as anticipated, while involved in a competition relationship. Why did the situation happen? RNA-seq revealed that the focal adhesion signaling pathway, the MAPK signaling pathway, the PI3K-AKT signaling pathway, and the NF-κB signaling pathway were significantly activated in the soft PDMS group. On the contrary, there were no differences between the soft group and the soft dot-array group, showing a weak regulation from surface topology. Based on the results of RNA-seq, WB, and immunofluorescence experiments, we concluded that the underlying mechanism of inflammatory responses induced by stiffness should be that focal adhesion activated AP-1 transcription factor at the late stage, which could further enhance the activity of NF-κB. Ultimately, this resulted in the upregulation of inflammatory cytokines,
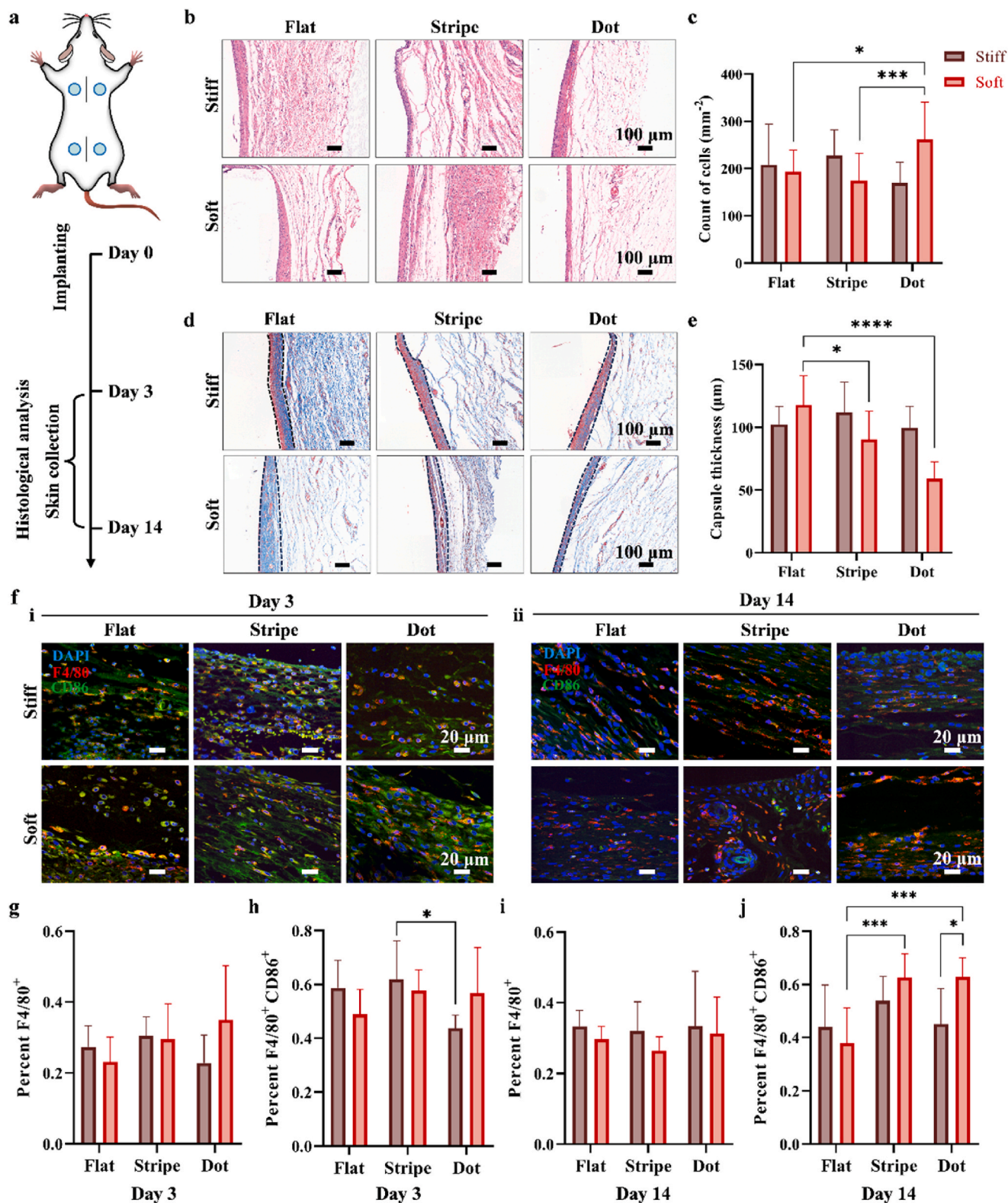
Fig. 5. *In vivo* **immune responses to various implants.** (**a**) Schematic of *in vivo* immune response experiments. (**b**) H&E staining images of skin tissues in the stiff and soft groups after implanting for 14 days. (**c**) Quantitative analysis of acute inflammatory responses after implanting for 14 days ($n = 3$). (**d**) Masson's trichrome staining images of skin tissues in the stiff and soft groups after implanting for 14 days. Black dash lines in the amplified images denote fibrous capsules. (**e**) Thickness of fibrous capsule in different groups after implanting for 14 days ($n = 3$). (**f**) Immunofluorescence images of M1 macrophages marked by F4/80 (blue) and CD86 (green) after implanting for 3 (i) and 14 (ii) days. (**g-j**) Percentage of F4/80$^+$ and F4/80$^+$CD86$^+$ cells of skin tissues on day 3 (g–h) and day 14 (i–j), corresponding to (f). Bars denote Mean ± SD, *$p < 0.05$, **$p < 0.01$, ***$p < 0.001$, ****$p < 0.001$ as determined by Two-way ANOVA and Tukey post-hoc test. (For interpretation of the references to colour in this figure legend, the reader is referred to the Web version of this article.)

including TNF-α, IL-6, and IL-1β.

In summary, this study exploring the inflammatory responses of M1 macrophages showed that there is a competitive relationship between stiffness and surface topology, with no synergistic effect observed. As the stiffness reaches the levels of MPa, stiffness dominates the regulation of the mechanical transduction of M1 macrophages, while surface topology plays a secondary role. The depression from surface topology largely depends on the stiffness of materials, because they mediate the same mechanical transduction molecules involving cytoskeleton [18,24]. Therefore, for hard implants, mechanical properties should be considered first during the design stage, to avoid adverse immune responses. Given the fibrosis level of the implants and the suppression of inflammatory responses, this revealed that soft dot-array PDMS should be the best candidate. Considering the characteristic size of macrophages is in the range of 10–30 μm, we designed the patterned structures to be in the size of 20–30 μm, which indeed worked as expected. Thus, we conclude that medical silicone implants should exhibit patterned structures in the tens-of-micrometers range.

This study also proved that the mechanical transduction of macrophages induced by stiffness and surface topology followed complicated laws. Moreover, a lot of interesting biology occurs at the levels of kPa, especially the Young's modulus of 1–300 kPa that can mimic the mechanical properties of skin and organs [49]. Many studies have discussed the inflammatory responses of M1 macrophages at the levels of kPa [34], which have shown that multiple mechanical sensors contribute to the inflammatory responses of M1 macrophages. Furthermore, lower stiffness can depress inflammatory responses at the levels of genes and proteins, and even weaken FBR. In contrast, our study mainly focused on the hard implants which showed a more complicated regulation rule, further revealing the complicated underlying mechanism of mechanical transduction of cells. We must denote that the regulation effect resulting from stiffness was more significant than stiffness at the levels of kPa. Besides, another interesting question can be raised: "Could surface topology play a more significant role when the substrate has stiffness at the levels of kPa?", which requires more investigation.

4. Materials and Experiments

4.1. Materials

PDMS (SYLGARD 184) was purchased from DOW Corning. Fibronectin (440 kDa) and Lipopolysaccharide (LPS) were purchased from Sigma-Aldrich. Interferon-γ (IFN-γ, Lot: c746), Interleukin-4 (IL-4, Lot: CH18), and Interleukin-13 (IL-13, Lot: CK15) were purchased from Novoprotein. Macrophage colony stimulating factor (M-CSF, Lot: 0521245) was purchased from PeproTech. Penicillin-Streptomycin Liquid (PS, Lot: 2309004) was purchased from Solarbio. Fetal Bovine Serum (FBS) was purchased from Hyclone. RNAiso Plus (Lot: 9109) was purchased from TaKaRa. HiScript III RT SuperMix (Lot: R323-01) and ChamQ Universal SYBR qPCR Master Mix (Lot: Q711) were purchased from Vazyme. Total Protein extraction kit (Lot: PE001) was purchased from SAB. Mouse Tnf-α ELISA kit (Lot: KE10002) and Mouse IL-6 ELISA kit (Lot: KE10007) were purchased from Proteintech. Primary antibodies of iNOS (Lot: ab178945) and F4/80 (Lot: ab300421) were purchased from Abcam. Primary antibodies of NF-κB p65 (Lot: 8242S) and Phospho-NF-κB (p65, Lot: 3033s) were purchased from Cell signaling technology. Primary antibody of CD86 (Lot: sc-28347) was purchased from Santa Cruz. Second antibody of Goat Anti-Rabbit IgG (H + L) (Cy3, red, Lot: A0516), Goat Anti-Mouse IgG(H + L) (Alexa Flour 488, green, Lot: A0428), and Antifade Mounting Medium with DAPI (Lot: P0131) and SDS-PAGE Sample Loading Buffer 5X (Lot: P0015L) were purchased from Beyotime. 488-conjugated Phalloidin antibody (Lot: PF00001) was purchased from Proteintech. The reagents for flow cytometry contained: anti-FcR (CD16/CD32) (Lot: 156603); APC-A700- conjugated CD86 (Lot: 1105024); FITC-conjugated CD206 (Lot: 141704) and propidium iodide solution (PI, Lot: 421301). These were purchased from Biolegend.

IC Fixation Buffer (Lot: 00-8222-49), Permeabilization Buffer (Lot: 00-8333-56), and Alex 488 conjugated iNOS (Lot: 53-5920-82).

4.2. Fabrication of PDMS substrates

Stiff and soft PDMS substrates were produced by mixing the base component and the curing component with ratios of 10 : 1 and 20 : 1. After stirring sufficiently, PDMS was centrifuged to remove bubbles for 5 min at 2000 rpm. The PDMS was poured onto a custom-patterned silicon wafer , a vacuum pump was used to remove air from the mixture. After the mixture was evenly distributed on the patterned silicon wafer, it was put into an oven at 70 °C for 2 h to get the solid PDMS.

4.3. Characterization of surface topology and mechanical property

Surface morphologies and topologies of PDMS substrates were captured by SEM (S-4800, Hitachi, Japan) and AFM (MultiMode 8, Bruker, USA). 3D surface topologies of PDMS substrates were characterized by the white light interferometer (Contour GT-K, Bruker, USA). The mechanical properties of PDMS were tested by the electromechanical universal testing machine (E44.304, MTS, USA), where PDMS samples were replicated from the dumbbell shape mold with $2 \times 4 \times 75$ mm^3. Young's modulus was calculated through the elastic regime of the stress–strain curve. The water contact angles of stiff and soft PDMS surfaces were measured by the contact angle instrument (SL150E, KINO, USA). The surface chemical components of PDMS substrates were analyzed by X-ray photoelectron spectroscopy (XPS) (Thermo Fisher Scientific, K-Alpha, USA).

4.4. Macrophages differentiation, culture, and activation

6 to 8-week-old C57BL/6 mice were used to obtain bone marrow-derived macrophages (BMDMs). BMDMs was flushed with PBS, which then was separated into a single-cell suspension by passing cell stainers in the pore size of 70 μm. 5×10^6 cells were seeded into 90 mm plastic dishes in 5 % CO$_2$ at 37 °C, during which culture medium was changed every 24 h for 7 days, where the culture medium contained RAMI-1640, 10 % FBS, 1 % PS, and 2 % M-CSF. BMDMs were used for next experiments on day 7.

Before seeding BMDMs on the targeted PDMS substrates, 10 μg/mL fibronectin was coated on the PDMS substrates for 30 min, and the PDMS substrates were washed three times with PBS. 1×10^6 BMDMs were seeded onto every PDMS substrate, and incubated for 24 h to ensure the complete adhesion of cells. Subsequently, pro-inflammatory M1 macrophages were induced by adding 20 ng/mL LPS and 10 ng/mL IFN-γ into the medium for 24 h. M1 macrophages were then used for subsequent experiments.

4.5. Quantitative real-time PCR (RT-qPCR)

Total RNA was isolated from BMDMs by using RNAiso Plus. The cDNA was synthesized from 500 ng total RNA using HiScript III RT SuperMix. The ChamQ Universal SYBR qPCR Master Mix was used to detect the gene expression. Results were analyzed by the $2^{-\Delta\Delta Ct}$ method and gene expressions were normalized to GAPDH. The forward and reverse primer sequences were presented in Table S2.

4.6. Immunofluorescence and semi-quantitative analysis

First, M1 macrophages on PDMS substrates were washed with PBS for three times. The cells were fixed with 4 % paraformaldehyde for 10 min at room temperature and next were washed three times with PBS. Subsequently, cells were permeabilized by 0.2 % Triton X-100 for 10 min and were washed with PBS as previously. Before incubating primary antibody iNOS (1 : 500), and NF-κB (p65, 1 : 500). 10 % goat serum was used to block nonspecific protein binding sites for 1 h at room

temperature. Primary antibody was added to each group, and incubated for overnight at 4 °C. After that, cells were washed as previously and then incubated with the secondary antibody (Red, 1 : 200), for 1 h at room temperature. The cytoskeleton was stained by phalloidin (Green, 1 : 400) for 20 min at room temperature. After completely washing, the nucleus was stained with an antifade mounting medium with DAPI. In the shape and morphological statistics of BMDMs, we defined the long axis as the longest length of the cell, and the short axis was perpendicular to the long axis and passed through the nucleus. Images were captured by LSCM (Olympus, Tokyo, Japan). Image processing and semi-quantitative analysis were performed using Olyvia (ver. 3.3, Olympus, Tokyo) and ImageJ (ver. 1.52, National Institutes of Health, Rockville, MD, USA).

4.7. Flow cytometry assay

The suspensions of BMDMs were collected by the treatment of trypsin, centrifugation, and resuspension processes. Then using anti-FcR (2 : 500) to block cells for 15 min at 4 °C, washed with PBS and incubated with APC-A700-conjugated CD86 (1 : 100), FITC-conjugated CD206 (1 : 100) and PI (2 : 50) for 30 min at room temperature. After being washed by PBS, the BMDMs would be resuspended again and then analyzed with a flow cytometer (Attune acoustic focusing cytometer, Thermo Fisher). After surface staining, cells got fixed and permeabilized, and were stained with Alex 488 conjugated iNOS antibody at 4 °C in the dark for 60 min. The control groups of M1 and M2 BMDMs were treated by LPS (20 ng/mL)/IFN-γ (10 ng/mL) and IL-4 (20 ng/mL)/IL-13 (20 ng/mL), respectively. Isotype controls were set in all groups, and every group was performed in triplicate. Data were analyzed by using FlowJo software (ver. 10.4).

4.8. Western blot analysis

For western blotting assay, BMDM were collected by the previous procedure. Total cell proteins were obtained by a protein extraction kit according to the provided protocol. Scraping the substrate to allow the cells to react fully with the lysis buffer. The lysate was centrifuged at 14,000 g for 15 min at 4 °C. Adding 5 × SDS loading buffer at a 1:4 ratio, then heat the mixture at 95 °C for 10 min to get protein sample. Protein samples were separated through a 10 % Bis-Tris polyacrylamide gel and transferred onto a PVDF membrane (0.45 μm). Using 5 % nonfat milk in TBST blocks the membrane for 2 h at room temperature. Then the membrane was incubated with rabbit monoclonal antibody to NF-κB p65 (1:1000) and Phospho-NF-κB p65 (1:1000) overnight at 4 °C. After that, the membranes were washed with TBST 3 times per 10 min and incubated with a goat anti-rabbit horseradish peroxidase-conjugated secondary antibody for 1 h at room temperature. Repeat the membrane washing step as previously described. The proteins on the membranes were visualized by Invitrogen iBright Imaging system (Thermo, USA). The signal intensity of immunoreactive bands were quantified by ImageJ.

4.9. Enzyme-linked immunosorbent assay (ELISA)

Collecting the culture supernatant after stimulating macrophages at the previous procedure for 24 h, centrifuge at 500 g for 5 min and use immediately. The concentrations of mouse inflammatory cytokines from BMDM culture supernatant samples were measured with IL-6 and TNF-α ELISA Kits according to the manufacturer's protocols.

4.10. RNA sequencing

Total RNA was extracted from each sample using TRIzol reagent, quantified, and purified with the Bioanalyzer 2100 and the RNA 6000 Nano LabChip Kit (Agilent, CA) according to the manufacturer's instructions. The RNA libraries were prepared and sequenced on an Illumina Novaseq™ 6000 platform (LC Bio Technology, Hangzhou, China). Data analysis and visualization were performed using the OmicStudio platform (LC Bio Technology, Hangzhou, China) and Cytoscape (ver. 3.9.1). The differential expression analysis was performed using DESeq2 software among different groups. Genes with q-value <0.05 and absolute fold change ≥2 were considered as significantly expressed genes.

4.11. Implanting experiments

6 week-old SD rats weighing 200–250 g were chosen for the implanting experiments. The dorsal skin of rats was shaved one day ahead of implantation. Before operating, the dorsal skin would be sterilized with 75 % ethanol. Four incisions about 1.5 cm parallel to the dorsal medium line were made as subcutaneous pockets, then each slice of PDMS would be placed in a single pocket. Patterned or unpatterned PDMS substrates were cut into slices with a diameter of 6 mm, which were sterilized by UV for 30 min. Eventually, the incision would be closed with surgical sutures effectively to avoid the emergence of dead space. SD rats were euthanized on days 3 and 14, and skin tissues including resident slices were fixed in 4 % paraformaldehyde for H&E staining, Masson's trichrome staining, and Immunofluorescence. All animal procedures were approved by the Animal Care and Use Committee of Army Medical University (AMUWEC20232425 and 20226004). All SD rats were acclimatized for 1 week before any experimental procedures.

4.12. Histological analysis

Skin tissues including PDMS were dehydrated, embedded in paraffin, and sectioned for histological analysis. According to standard instruction, H&E (hematoxylin and eosin) staining, Masson's trichrome staining, and Immunofluorescence were performed. All histological Images were analyzed with Slide Viewer (ver. 2.7, 3D Histech) and ImageJ software.

4.13. Inflammation evaluation

Slides containing complete tissue structures were chosen for H&E staining to quantify tissue inflammation. In the inflammation evaluation, fields of view were randomly selected from each slide to estimate the local inflammation by counting infiltrating cells in the area near the implant. Each group selected more than 8 fields of view with 40 × , and each group was analyzed with 3 independent samples. Only slides with intact tissues were selected for statistics. The evaluation of inflammation was performed using ImageJ for semi-quantitative analysis of inflammation by infiltrating cell counts [27].

4.14. Collagen density and capsule thickness measurement

Masson's trichrome staining was used to evaluate collagen density and capsule thickness. The capsule region was measured directly by Slide Viewer. To analyze collagen density, measure the area of blue-stained collagen in the images after applying a uniform threshold to all slides using the ImageJ software. Next, divide the boxed area by the total area to obtain the percentage. Each group contains at least 12 fields of view with 40 × . These images were selected randomly and analyzed with 3 independent samples [21].

4.15. Immunofluorescence of paraffin-embedded slices

Slices were deparaffinized first, then antigen retrieval was performed using sodium citrate solution, washed 5 times in PBS for 3 min each, and permeabilized with 0.2 % Triton X-100. Block for 2 h at room temperature using 10 % goat serum. Slices were incubated with Primary antibody F4/80 (1:400) and CD86 (1:200) overnight at 4 °C. Wash 5 times in

PBS for 3 min each, then add the corresponding secondary antibody and incubate for 1 h at room temperature in the dark. Repeat the washing steps above. After being mounted with an antifade mounting medium with DAPI, CLSM obtained images. Every group has at least 9 images, these images were evaluated by using ImageJ.

4.16. Statistical analysis

The data here was presented as mean $\pm$ standard deviation and analyzed by GraphPad Prism (ver. 9.3). Significance between the two groups was performed by a two-tailed t-test. The rest of the statistical analyses were performed by Two-way ANOVA (or mixed model) and Tukey post-hoc test. A value of $p < 0.05$ was considered statistically significant (*$p < 0.05$, **$p < 0.01$, ***$p < 0.001$, ****$p < 0.0001$).

CRediT authorship contribution statement

Sicen He: Writing – review & editing, Writing – original draft, Visualization, Validation, Methodology, Investigation. **Qingrong Zhang:** Writing – original draft, Visualization, Validation, Methodology. **Jiezhi Jia:** Validation, Methodology. **Wei Xia:** Validation, Methodology. **Shengnan Chen:** Validation, Methodology. **Fanyi Min:** Validation, Methodology. **Yanlin Song:** Methodology. **Yunlong Yu:** Writing – review & editing, Supervision. **Jiangfeng Li:** Writing – review & editing, Supervision. **Zheng Li:** Writing – review & editing, Visualization, Validation, Methodology, Data curation, Conceptualization. **Gaoxing Luo:** Writing – review & editing, Supervision, Project administration, Funding acquisition.

Declaration of competing interest

The authors declare that they have no known competing financial interests or personal relationships that could have appeared to influence the work reported in this paper.

Acknowledgments

Appendix A. Supplementary data

Supplementary data to this article can be found online at https://doi.org/10.1016/j.mtbio.2024.101304.

Data availability

Data will be made available on request.

References

[1] A.J.T. Teo, A. Mishra, I. Park, Y.J. Kim, W.T. Park, Y.J. Yoon, Polymeric biomaterials for medical implants and devices, ACS Biomater. Sci. Eng. 2 (4) (2016) 454–472.

[2] A.W. Lloyd, R.G. Faragher, S.P. Denyer, Ocular biomaterials and implants, Biomaterials 22 (8) (2001) 769–785.

[3] P.J. VandeVord, N. Gupta, R.B. Wilson, R.Z. Vinuya, C.J. Schaefer, A.I. Canady, P. H. Wooley, Immune reactions associated with silicone-based ventriculo-peritoneal shunt malfunctions in children, Biomaterials 25 (17) (2004) 3853–3860.

[4] A. Gabriel, G.P. Maxwell, The evolution of breast implants, Clin. Plast. Surg. 42 (4) (2015) 399–404.

[5] A. Lamberti, S.L. Marasso, M. Cocuzza, PDMS membranes with tunable gas permeability for microfluidic applications, RSC Adv. 4 (106) (2014) 61415–61419.

[6] J.C. Doloff, O. Veiseh, R. de Mezerville, M. Sforza, T.A. Perry, J. Haupt, M. Jamiel, C. Chambers, A. Nash, S. Aghlara-Fotovat, J.L. Stelzel, S.J. Bauer, S.Y. Neshat, J. Hancock, N.A. Romero, Y.E. Hidalgo, I.M. Leiva, A.M. Munhoz, A. Bayat, B. M. Kinney, H.C. Hodges, R.N. Miranda, M.W. Clemens, R. Langer, The surface topography of silicone breast implants mediates the foreign body response in mice, rabbits and humans, Nat. Biomed. Eng. 5 (10) (2021) 1115–1130.

[7] R. Klopfleisch, F. Jung, The pathology of the foreign body reaction against biomaterials, J. Biomed. Mater. Res. 105 (3) (2017) 927–940.

[8] A.H. Morris, T.R. Kyriakides, Matricellular proteins and biomaterials, Matrix Biol. : journal of the International Society for Matrix Biology 37 (2014) 183–191.

[9] C.J. Coroneos, J.C. Selber, A.C. Offodile 2nd, C.E. Butler, M.W. Clemens, US FDA breast implant postapproval studies: long-term outcomes in 99,993 patients, Ann. Surg. 269 (1) (2019) 30–36.

[10] T. ten Brink, F. Damanik, J.I. Rotmans, L. Moroni, Unravelling & harnessing the immune response at the cell-biomaterial interface for tissue engineering purposes, Adv. Healthcare Mater. 13 (2024) e2301939.

[11] J.S. Duffield, M. Lupher, V.J. Thannickal, T.A. Wynn, Host responses in tissue repair and fibrosis, Annual review of pathology 8 (2013) 241–276.

[12] S. Liu, Q. Zhang, J. Yu, N. Shao, H. Lu, J. Guo, X. Qiu, D. Zhou, Y. Huang, Absorbable thioether grafted hyaluronic acid nanofibrous hydrogel for synergistic modulation of inflammation microenvironment to accelerate chronic diabetic wound healing, Adv. Healthcare Mater. 9 (11) (2020) e2000198.

[13] Z. Tu, M. Chen, M. Wang, Z. Shao, X. Jiang, K. Wang, Z. Yao, S. Yang, X. Zhang, W. Gao, C. Lin, B. Lei, C. Mao, Engineering bioactive M2 macrophage-polarized anti-inflammatory, antioxidant, and antibacterial scaffolds for rapid angiogenesis and diabetic wound repair, Adv. Funct. Mater. 31 (30) (2021).

[14] X. Wu, W. He, X. Mu, Y. Liu, J. Deng, Y. Liu, X. Nie, Macrophage polarization in diabetic wound healing, Burns & trauma 10 (2022).

[15] F.O.S.G. Martinez, The M1 and M2 paradigm of macrophage activation: time for reassessment, F1000 Prime Rep 6 (2014) 13.

[16] N. Erathodiyil, H.-M. Chan, H. Wu, J.Y. Ying, Zwitterionic polymers and hydrogels for antibiofouling applications in implantable devices, Mater. Today 38 (2020) 84–98.

[17] D. Zhang, Q. Chen, C. Shi, M. Chen, K. Ma, J. Wan, R. Liu, Dealing with the foreign-body response to implanted biomaterials: strategies and applications of new materials, Adv. Funct. Mater. 31 (6) (2021).

[18] N. Noskovicova, R. Schuster, S. van Putten, M. Ezzo, A. Koehler, S. Boo, N. M. Coelho, D. Griggs, P. Ruminski, C.A. McCulloch, B. Hinz, Suppression of the fibrotic encapsulation of silicone implants by inhibiting the mechanical activation of pro-fibrotic TGF-β, Nat. Biomed. Eng. 5 (12) (2021) 1437–1456.

[19] B.D. Ratner, Healing with medical implants: the body battles back, Sci. Transl. Med. 7 (272) (2015) 272fs4.

[20] H. Yan, C. Seignez, M. Hjorth, B. Winkeljann, M. Blakeley, O. Lieleg, M. Phillipson, T. Crouzier, Immune-informed mucin hydrogels evade fibrotic foreign body response in vivo, Adv. Funct. Mater. 29 (46) (2019) 1902581.

[21] D. Zhang, Q. Chen, Y. Bi, H. Zhang, M. Chen, J. Wan, C. Shi, W. Zhang, J. Zhang, Z. Qiao, J. Li, S. Chen, R. Liu, Bio-inspired poly-DL-serine materials resist the foreign-body response, Nat. Commun. 12 (1) (2021) 5327.

[22] S. Camarero-Espinosa, M. Carlos-Oliveira, H. Liu, J.F. Mano, N. Bouvy, L. Moroni, 3D printed dual-porosity scaffolds: the combined effect of stiffness and porosity in the modulation of macrophage polarization, Adv. Healthcare Mater. 11 (1) (2022) 2101415.

[23] W. Liu, Q. Sun, Z.L. Zheng, Y.T. Gao, G.Y. Zhu, Q. Wei, J.Z. Xu, Z.M. Li, C.S. Zhao, Topographic cues guiding cell polarization via distinct cellular mechanosensing pathways, Small 18 (2) (2022) 2104328.

[24] N. Jain, V. Vogel, Spatial confinement downsizes the inflammatory response of macrophages, Nat. Mater. 17 (12) (2018) 1134–1144.

[25] F.Y. McWhorter, T.T. Wang, P. Nguyen, T. Chung, W.F. Liu, Modulation of macrophage phenotype by cell shape, Proc. Natl. Acad. Sci. U. S. A. 110 (43) (2013) 17253–17258.

[26] A.G. Solis, P. Bielecki, H.R. Steach, L. Sharma, C.C.D. Harman, S. Yun, M.R. de Zoete, J.N. Warnock, S.D.F. To, A.G. York, M. Mack, M.A. Schwartz, C.S. Dela Cruz, N.W. Palm, R. Jackson, R.A. Flavell, Mechanosensation of cyclical force by PIEZO1 is essential for innate immunity, Nature 573 (7772) (2019) 69–74.

[27] V.S. Meli, H. Atcha, P.K. Veerasubramanian, R.R. Nagalla, T.U. Luu, E.Y. Chen, C. F. Guerrero-Juarez, K. Yamaga, W. Pandori, J.Y. Hsieh, T.L. Downing, D. A. Fruman, M.B. Lodoen, M.V. Plikus, W. Wang, W.F. Liu, YAP-mediated mechanotransduction tunes the macrophage inflammatory response, Sci. Adv. 6 (49) (2020) eabb8471.

[28] M. Huse, Mechanical forces in the immune system, Nat. Rev. Immunol. 17 (11) (2017) 679–690.

[29] H. Du, J.M. Bartleson, S. Butenko, V. Alonso, W.F. Liu, D.A. Winer, M.J. Butte, Tuning immunity through tissue mechanotransduction, Nat. Rev. Immunol. 23 (3) (2023) 174–188.

[30] V.F. Achterberg, L. Buscemi, H. Diekmann, J. Smith-Clerc, H. Schwengler, J. J. Meister, H. Wenck, S. Gallinat, B. Hinz, The nano-scale mechanical properties of the extracellular matrix regulate dermal fibroblast function, J. Invest. Dermatol. 134 (7) (2014) 1862–1872.

[31] Y.Z. Zhu, H. Liang, X.M. Liu, J. Wu, C. Yang, T.M. Wong, K.Y.H. Kwan, K.M. C. Cheung, S.L. Wu, K.W.K. Yeung, Regulation of macrophage polarization through surface topography design to facilitate implant-to-bone osteointegration, Sci. Adv. 7 (14) (2021) eabf6654.

[32] D. Dong, C. Tsao, H.C. Hung, F. Yao, C. Tang, L. Niu, J. Ma, J. MacArthur, A. Sinclair, K. Wu, P. Jain, M.R. Hansen, D. Ly, S.G. Tang, T.M. Luu, P. Jain, S. Jiang, High-strength and fibrous capsule-resistant zwitterionic elastomers, Sci. Adv. 7 (1) (2021) eabc5442.

[33] T. Zheng, L. Wu, S. Sun, J. Xu, Q. Han, Y. Liu, R. Wu, G. Li, Co-culture of Schwann cells and endothelial cells for synergistically regulating dorsal root ganglion behavior on chitosan-based anisotropic topology for peripheral nerve regeneration, Burns & trauma 10 (2022) tkac030.

[34] M.P. Lin, H.Y. Wang, C.S. Ruan, J. Xing, J.F. Wang, Y.L. Wang, Y.F. Luo, Adsorption force of fibronectin on various surface chemistries and its vital role in osteoblast adhesion, Biomacromolecules 16 (3) (2015) 973–984.

[35] S. Jiao, C. Li, F. Guo, J. Zhang, H. Zhang, Z. Cao, W. Wang, W. Bu, M. Lin, J. Lü, Z. Zhou, SUN1/2 controls macrophage polarization via modulating nuclear size and stiffness, Nat. Commun. 14 (1) (2023) 6416.

[36] X. Zheng, L. Xin, Y. Luo, H. Yang, X. Ye, Z. Mao, S. Zhang, L. Ma, C. Gao, Near-infrared-triggered dynamic surface topography for sequential modulation of macrophage phenotypes, ACS Appl. Mater. Interfaces 11 (46) (2019) 43689–43697.

[37] H. Atcha, A. Jairaman, J.R. Holt, V.S. Meli, R.R. Nagalla, P.K. Veerasubramanian, K.T. Brumm, H.E. Lim, S. Othy, M.D. Cahalan, M.M. Pathak, W.F. Liu, Mechanically activated ion channel Piezo1 modulates macrophage polarization and stiffness sensing, Nat. Commun. 12 (1) (2021) 3256.

[38] A. Saraswathibhatla, D. Indana, O. Chaudhuri, Cell-extracellular matrix mechanotransduction in 3D, Nat. Rev. Mol. Cell Biol. 24 (7) (2023) 495–516.

[39] O. Chaudhuri, J. Cooper-White, P.A. Janmey, D.J. Mooney, V.B. Shenoy, Effects of extracellular matrix viscoelasticity on cellular behaviour, Nature 584 (7822) (2020) 535–546.

[40] R. Sheng, J. Liu, W. Zhang, Y. Luo, Z. Chen, J. Chi, Q. Mo, M. Wang, Y. Sun, C. Liu, Y. Zhang, Y. Zhu, B. Kuang, C. Yan, H. Liu, L.J. Backman, J. Chen, Material stiffness in cooperation with macrophage paracrine signals determines the tenogenic differentiation of mesenchymal stem cells, Adv. Sci. 10 (17) (2023) e2206814.

[41] Y. Ni, H. Qi, F. Zhang, S. Jiang, Q. Tang, W. Cai, W. Mo, R.J. Miron, Y. Zhang, Macrophages modulate stiffness-related foreign body responses through plasma membrane deformation, Proc. Natl. Acad. Sci. U. S. A. 120 (3) (2023) e2213837120.

[42] T. Jayakumar, K.C. Lin, C.C. Chang, C.W. Hsia, M. Manubolu, W.C. Huang, J. R. Sheu, C.H. Hsia, Targeting MAPK/NF-κB pathways in anti-inflammatory

[43] potential of rutaecarpine: impact on src/FAK-mediated macrophage migration, Int. J. Mol. Sci. 23 (1) (2021) 92.

[43] S.E. Byeon, Y.S. Yi, J. Oh, B.C. Yoo, S. Hong, J.Y. Cho, The role of Src kinase in macrophage-mediated inflammatory responses, Mediat. Inflamm. 2012 (2012) 512926.

[44] J.C. Doloff, O. Veiseh, A.J. Vegas, H.H. Tam, S. Farah, M. Ma, J. Li, A. Bader, A. Chiu, A. Sadraei, S. Aresta-Dasilva, M. Griffin, S. Jhunjhunwala, M. Webber, S. Siebert, K. Tang, M. Chen, E. Langan, N. Dholokia, R. Thakrar, M. Qi, J. Oberholzer, D.L. Greiner, R. Langer, D.G. Anderson, Colony stimulating factor-1 receptor is a central component of the foreign body response to biomaterial implants in rodents and non-human primates, Nat. Mater. 16 (6) (2017) 671–680.

[45] A. Isomursu, K.Y. Park, J. Hou, B. Cheng, M. Mathieu, G.A. Shamsan, B. Fuller, J. Kasim, M.M. Mahmoodi, T.J. Lu, G.M. Genin, F. Xu, M. Lin, M.D. Distefano, J. Ivaska, D.J. Odde, Directed cell migration towards softer environments, Nat. Mater. 21 (9) (2022) 1081–1090.

[46] M.M. Smoak, K.J. Hogan, K.J. Grande-Allen, A.G. Mikos, Bioinspired electrospun dECM scaffolds guide cell growth and control the formation of myotubes, Sci. Adv. 7 (20) (2021) eabg4123.

[47] Y. Li, X. Bi, M. Wu, X. Chen, W. Zhan, Z. Dong, F. Lu, Adjusting the stiffness of a cell-free hydrogel system based on tissue-specific extracellular matrix to optimize adipose tissue regeneration, Burns & trauma 11 (2023) tkad002.

[48] Y. Zhang, Y. Song, J. Du, W. Liu, C. Dong, Z. Huang, Z. Zhang, L. Yang, T. Wang, S. Xiong, L. Dong, Y. Guo, J. Dang, Q. He, Z. Yu, X. Ma, S100 calcium-binding protein A9 promotes skin regeneration through toll-like receptor 4 during tissue expansion, Burns & trauma 11 (2023) tkad030.

[49] A.J. Engler, S. Sen, H.L. Sweeney, D.E. Discher, Matrix elasticity directs stem cell lineage specification, Cell 126 (4) (2006) 677–689.